

A microphysical parameterization for convective clouds in the ECHAM5 climate model: Single-column model results evaluated at the Oklahoma Atmospheric Radiation Measurement Program site

Junhua Zhang¹ and Ulrike Lohmann²

Department of Physics and Atmospheric Science, Dalhousie University, Halifax, Nova Scotia, Canada

Philip Stier

Max Planck Institute for Meteorology, Hamburg, Germany

Received 14 June 2004; revised 20 September 2004; accepted 13 October 2004; published 17 May 2005.

[1] The microphysical parameterization used for stratiform clouds in the ECHAM5 climate model is now extended for simulations of convective clouds. The performance of the newly implemented parameterization in simulating midlatitude continental summertime convective cloud systems is evaluated in this paper at the Atmospheric Radiation Measurement Program (ARM) Southern Great Plains (SGP) site in Oklahoma using the single-column mode (SCM) of ECHAM5. Three ARM intensive operating periods (IOPs), including two summer ones and a late spring one, are used for the evaluation. Results show that the SCM simulated cloud cover fraction agrees well with observations. The SCM also captures most of the precipitation events. With the new microphysical parameterization, the model performs at least as well as with the original model setup in simulating almost all the fields examined in this study. Significant improvement is shown in the simulations of outgoing longwave radiation and net incoming solar radiation at the top of the atmosphere revealing the feasibility of the new parameterization. Sensitivity studies show that a 10-fold increase in cloud droplet number concentration significantly increases the simulated liquid water content. More interestingly, this increase in cloud droplet number leads to an increase in the total amount of precipitation in two of the three IOPs.

Citation: Zhang, J., U. Lohmann, and P. Stier (2005), A microphysical parameterization for convective clouds in the ECHAM5 climate model: Single-column model results evaluated at the Oklahoma Atmospheric Radiation Measurement Program site, *J. Geophys. Res.*, 110, D15S07, doi:10.1029/2004JD005128.

1. Introduction

[2] Convective clouds play an important role in the atmospheric system by transporting large amounts of energy and water vapor from the surface to the free troposphere. In this process, they produce large amounts of precipitation and drive the global-scale circulation. Properly representing convective clouds in a general circulation model (GCM) is a very important issue for conducting global climate simulations. Aerosol effects on clouds and climate is another important process that influences the global climate through the direct aerosol effect [e.g., Hobbs *et al.*, 1997], indirect aerosol effect [e.g., Lohmann and Feichter, 1997; Lohmann

et al., 2000] and semidirect aerosol effect [e.g., Ackerman *et al.*, 2000]. However, the understanding of aerosol effects on climate is still in its infancy, especially for the indirect effect which has the largest uncertainty among all the external factors addressed in IPCC report [Ramaswamy *et al.*, 2001]. So far, aerosol effects on clouds are mainly studied in the framework of large-scale stratiform clouds in climate models [e.g., Lohmann and Feichter, 1997; Roelofs *et al.*, 1998; Penner *et al.*, 1998; Lohmann *et al.*, 2000; Rotstayn *et al.*, 2000; Peng and Lohmann, 2003]. Nevertheless, observations show that aerosol effects on precipitation formation in deep convective clouds maybe important [e.g., Rosenfeld and Lensky, 1998; Rosenfeld, 1999, 2000]. Using a bin-microphysical cloud model, Khain *et al.* [2001] reproduced aircraft observations of supercooled water in convective cloud down to -37.5°C if a high concentration of cloud condensation nuclei (CCN) is introduced. In climate models, however, the effects of aerosols on convective cloud are only starting to be addressed [Nobler *et al.*, 2003]. This is partly due to the difficulty of representing small-scale convective clouds in the large grid boxes of the climate model, and partly due to the rather simple cloud

¹Now at Modelling and Integration Division (ARQI), Air Quality Research Branch, Meteorological Service of Canada, Downsview, Ontario, Canada.

²Now at Institute for Atmospheric and Climate Science, Eidgenossische Technische Hochschule (ETH), Zurich, Switzerland.

microphysical processes currently used for convective clouds in GCMs.

[3] Using a cloud-resolving convection parameterization approach (also called “superparameterization”), *Grabowski* [2003] found that the cloud microphysics can significantly affect the quasi-equilibrium temperature and moisture profiles, which revealed the importance of microphysical parameterization for convective clouds in climate models. *Nober et al.* [2003] studied the aerosol effect on convective clouds in the ECHAM4 GCM by simply decreasing the conversion rate of cloud water to precipitation to 25% of the original rate for a cloud droplet number concentration (CDNC) between 750 cm^{-3} and 1000 cm^{-3} , and totally suppressing precipitation when CDNC exceeds 1000 cm^{-3} . With this assumption, they found a definite perturbation of the global circulation. However, cloud-resolving model simulations reveal that the increase in CDNC can result in increasing precipitation for convective systems in either tropical oceanic or midlatitude continental environments [*Khain et al.*, 2005; *Tao et al.*, 2004]. This, however, does not seem to be in agreement with recent observations that biomass burning could suppress cloud and rainfall processes [*Andreae et al.*, 2004]. Mesoscale simulations also show that a 10-fold increase of CDNC can lead to an increase in accumulated snow when a certain crystal shape (aggregates) is assumed [*Lohmann et al.*, 2003].

[4] In the recent ECHAM5 GCM [*Roeckner et al.*, 2003], a cloud microphysical parameterization [*Lohmann and Roeckner*, 1996] is applied for stratiform clouds, in which cloud liquid water and cloud ice are prognostic variables. In this study, we will implement this stratiform cloud microphysical parameterization into the convective cloud scheme and evaluate its performance by simulating the midlatitude continental summertime convective cloud systems at the Atmospheric Radiation Measurement (ARM) Southern Great Plain (SGP) site using the single-column mode (SCM) of ECHAM5. The emphasis of this study is to show the feasibility of using a more realistic microphysical parameterization for convective clouds in order to study aerosol effects on convective clouds rather than to improve the model simulations. Nevertheless, the performance of the model is evaluated by comparing the model simulations with observational data.

[5] The description of the convective scheme and the microphysical parameterization used for stratiform clouds in ECHAM5 is in the following section and the implementation of the parameterization is described in section 3. Results of the SCM simulations are discussed in section 4 and conclusions are given in section 5.

2. Model Description

2.1. Convective Scheme

[6] In ECHAM 5, the cumulus parameterization is based on the mass flux scheme by *Tiedtke* [1989] as discussed in the work of *Deutsches Klimarechenzentrum (DKRZ)* [1993] (see also <http://www.mpimet.mpg.de/en/extra/models/echam/index.php>) with modifications for penetrative convection according to *Nordeng* [1994]. In this assumption, cumulus clouds are considered to be embedded in the large-scale environment with a common cloud base but different vertical extents. They are defined by an upward and

downward mass flux, and by the heat, moisture and cloud water content. The scheme treats the bulk properties of cumulus updrafts and downdrafts separately. The bulk properties, such as cloud base mass flux and entrainment/detrainment rates are specified differently for penetrative, midlevel and shallow convection.

[7] Two types of entrainment of mass into convective plumes are considered: turbulent exchange of mass through the cloud edges and through organized inflow associated with large-scale convergence. Detrainment due to turbulent exchange and by organized outflow at cloud top are also assumed. Organized entrainment takes place when the buoyancy is positive. Organized detrainment takes place where the air decelerates, i.e., when the buoyancy becomes negative. It is defined as the loss of total mass flux due to detrainment of those clouds which are losing their buoyancy. A detailed description of this mass flux scheme can be found in the work of *Tiedtke* [1989], *DKRZ* [1993], and *Roeckner et al.* [2003].

[8] Condensation of water vapor to form cloud water and the formation of convective precipitation are considered in the updrafts. The bulk equation for cloud water in the updraft region of the cloud is defined as [*Tiedtke*, 1989; *DKRZ*, 1993; *Roeckner et al.*, 2003]:

$$\frac{\partial(M_u l)}{\partial z} = -D_u l + \bar{\rho} c_u - \bar{\rho} G_p \quad (1)$$

where M_u is the upward mass flux, D_u is the mass detrainment rate. l , $\bar{\rho}$, c_u , G_p are the cloud water content, air density, net condensation, and conversion rate from cloud water to precipitation, respectively, in the updraft region. Overbar denotes average over the horizontal area. The cloud water detrainment in equation (1) is used as a source term in the stratiform cloud water and ice equations (equations (5) and (6)).

[9] Precipitation formed in updraft clouds is crudely represented in the standard scheme as discussed in the work of *Tiedtke* [1989] and *DKRZ* [1993]. It is proportional to the cloud water content:

$$\bar{\rho} G_p = M_u K(p) l \quad (2)$$

where $K(p)$ is an empirical function that varies with pressure p . To ensure that no precipitation is produced in shallow convective clouds, $K(p)$ is assumed to be zero in a Δp_{crit} range above the cloud base and remains constant at higher levels as defined in equation (3), following *Tiedtke* [1989] and *DKRZ* [1993]:

$$K(p) \begin{cases} 0 & p_B - p \leq \Delta p_{crit} \\ 6 \times 10^{-4} m^{-1} & p_B - p > \Delta p_{crit} \end{cases} \quad (3)$$

here p_B is the pressure at cloud base and Δp_{crit} is the critical pressure range for precipitation formation, it is set to 150 hPa over ocean and 300 hPa over land. The net condensed cloud water content l_{cond} is calculated as the amount of water vapor that exceeds the saturation specific humidity:

$$l_{cond} = q - q_s \quad (4)$$

where q is the specific humidity and q_s is the saturation specific humidity over water or ice depending on the

temperature, T . If $T \geq 0^\circ\text{C}$, the saturation specific humidity is assumed to be with respect to water, otherwise, it is with respect to ice.

[10] Downdrafts are considered to be associated with convective precipitation from the updrafts and originate from cloud air influenced by the injection of environmental air. As described in the work of *Fritsch and Chappell* [1980] and *Foster* [1958], the level of free sinking (LFS) is assumed to be the highest model level where a mixture of equal parts of cloud air and saturated environmental air at wet-bulb temperature becomes negatively buoyant with respect to the environmental air. The downward mass flux is assumed to be directly proportional to the upward mass flux. In the downdrafts, some rain and snow is evaporated/sublimated to maintain a saturated descent. The environmental air injected at LFS is moisturized and cooled by the evaporation of precipitation. Detailed description of downdraft mass flux can also be found in the work of *Tiedtke* [1989] and *DKRZ* [1993].

[11] The vertical structure of the model is shown as in the work of *Tiedtke* [1989, Figure 1]. The ascent of cloud water in the updraft is obtained by vertical integration of equation (1) layer by layer starting near the surface at the lowest condensation level which is determined from an adiabatic ascent. The cloud profile above cloud base is determined layer by layer by first calculating a dry adiabatic ascent with entrainment and detrainment included and then adjusting temperature and moisture toward a saturated state. Cloud top is the level where buoyancy is negative. Details of the discretization and integration of the model equations for cumulus parameterization are described by *Tiedtke* [1989].

2.2. Microphysical Parameterization for Stratiform Cloud

[12] The microphysical parameterization for stratiform clouds is based on *Lohmann and Roeckner* [1996] with some modifications [*Roeckner et al.*, 2003]. Parameterized microphysical processes are condensational growth of cloud droplets, depositional growth of ice crystals, homogeneous and heterogeneous freezing of cloud droplets, autoconversion of cloud droplets, aggregation of ice crystals, accretion of cloud droplets by rain, accretion of ice crystals and cloud droplets by snow, evaporation of liquid water and rain, sublimation of ice crystals and snow, melting of ice crystals and snow.

[13] As in the work of *Lohmann and Roeckner* [1996], the governing equations for the mass mixing ratios of cloud water (q_l) and cloud ice (q_i) are:

$$\frac{\partial q_l}{\partial t} = R(q_l) + b(Q_{cnd}^c - Q_{aut}^c - Q_{racl}^c - Q_{sac1}^c - Q_{fho}^c - Q_{fhe}^c + Q_{mti}^c) + (1-b)Q_{cnd}^o \quad (5)$$

$$\frac{\partial q_i}{\partial t} = R(q_i) + b(Q_{dep}^c - Q_{agg}^c - Q_{saci}^c + Q_{fho}^c + Q_{fhe}^c - Q_{mti}^c) + (1-b)Q_{dep}^o \quad (6)$$

where $R(\dots)$ denotes the sum over all transport terms of q_l and q_i , respectively, including advection of cloud water, turbulence and detrainment from convection, and b is the fractional cloud cover diagnosed from a probability

distribution functions (PDF) based cloud cover scheme [*Tompkins*, 2002]. The superscripts (c) and (o) refer to the cloudy and cloud-free part of the grid box, respectively. Q_{cnd}^c and Q_{dep}^c are condensation (evaporation) of cloud water and deposition (sublimation) of cloud ice in the cloudy part; Q_{cnd}^o and Q_{dep}^o are evaporation of cloud water and sublimation of cloud ice transported into the cloud-free part of a grid box; Q_{aut}^c and Q_{agg}^c are autoconversion of cloud droplets and aggregation of ice crystals; Q_{racl}^c , Q_{sac1}^c and Q_{saci}^c are accretion of cloud droplets by raindrops, by snow flakes and accretion of ice crystals by snow flakes; Q_{fho}^c and Q_{fhe}^c are homogeneous, and heterogeneous freezing of cloud droplets; and Q_{mti}^c is melting of ice crystals.

3. Implementation of the Microphysical Parameterization

[14] *Tiedtke* [1993] mentioned that the representation of cloud formation by convection is rather straightforward if cumulus convection is parameterized by means of a mass flux scheme because the source terms for the cloud fields can be readily expressed in terms of available model parameters. Following the separate treatment of cloud water and ice in the stratiform cloud parameterization, the bulk equation for cloud water in convective clouds, equation (1), can be separated as:

$$\frac{\partial(M_u q_l)}{\partial z} = -D_u q_l + \bar{\rho} c_{ul} - \bar{\rho} G_{pl} \quad (7)$$

$$\frac{\partial(M_u q_i)}{\partial z} = -D_u q_i + \bar{\rho} c_{ui} - \bar{\rho} G_{pi} \quad (8)$$

Where q_l , c_{ul} , G_{pl} , q_i , c_{ui} and G_{pi} represent cloud liquid water, condensation of water vapor, formation of rain from cloud water, cloud ice, deposition of water vapor and formation of snow from cloud ice, respectively. Details of how to parameterize these processes using the terms described in equations (5) and (6) are discussed below.

[15] Transport of convective clouds is not considered currently, thus $R(q_l)$ and $R(q_i)$ are set to zero. In ECHAM5, convection is treated in a column ignoring slantwise convection, but cloud water and ice can be transported out of the column by detrainment. Once cloud water is transported out of the column, it is treated as a source of large-scale cloud water content. Therefore the evaporation and sublimation terms in the cloud free part Q_{cnd}^o and Q_{dep}^o are not considered for convective clouds.

[16] Condensation and deposition (Q_{cnd}^c and Q_{dep}^c) are calculated by equation (4). However, the saturation specific humidity q_s is defined differently. If $T \geq 0^\circ\text{C}$, q_s is assumed to be with respect to water. If $T < -35^\circ\text{C}$, it is with respect to ice. Between these two temperatures, it depends on the ice water content in clouds in such a way that first cloud water is formed by condensation of water vapor and q_s is calculated with respect to water; then cloud ice can be formed by heterogeneous freezing of cloud water (equation (9)). If the cloud ice mixing ratio exceeds a threshold value (set to 0.5 mg kg^{-1}), the Bergeron-Findeisen process sets in allowing the ice crystals to grow at the

expense of cloud droplets. Further condensational growth of cloud droplets is inhibited because the water vapor is now deposited onto the ice crystals and q_s is therefore taken to be with respect to ice.

[17] All ice crystal melt (Q_{melt}^c) when the temperature is above 0°C. At temperatures below -35°C, the total amount of cloud water freezes homogeneously and instantaneously to cloud ice through the homogeneous freezing process (Q_{fho}^c). This assumption is consistent with many in situ observations [e.g., *Boudala et al.*, 2002]. Heterogeneous freezing of cloud droplets (Q_{fhe}^c) between 0°C and -35°C is parameterized by extrapolating *Bigg's* [1953] equation down to the cloud droplet size [*Murakami*, 1990; *Levkov et al.*, 1992]:

$$Q_{fhe}^c = a_1 \{ \exp[b_1(T_0 - T)] - 1 \} \frac{\rho q_{cl}^2}{\rho_l N_l} \quad (9)$$

Where $a_1(=100 \text{ m}^{-3} \text{ s}^{-1})$ and $b_1(=0.66 \text{ K}^{-1})$ are determined from laboratory experiments. ρ is the air density and $\rho_l(=1000 \text{ kg m}^{-3})$ is the density of water, T is the temperature and $T_0 = 273.16 \text{ K}$, q_{cl} is the cloud water mixing ratio in the cloudy part of the grid box ($q_{cl} = q_l/b$), and N_l is the cloud droplet number concentration.

[18] As discussed in section 2.1, the convective precipitation diagnosed in the standard convection scheme (equation (2)) depends linearly on the cloud water content. To prohibit precipitation in shallow convection, the constant factor $K(p)$ is arbitrarily constrained by equation (3). A more realistic treatment of precipitation formation, however, is applied for large-scale clouds in which precipitation is formed by the autoconversion and aggregation processes (Q_{aut}^c and Q_{agg}^c). The autoconversion rate depends highly nonlinearly on the cloud water content [*Beheng*, 1994]:

$$Q_{aut} = \left(\gamma_1 * 6 * 10^{28} n^{-1.7} (10^{-6} N_l)^{-3.3} (10^{-3} \rho q_{cl})^{4.7} \right) / \rho \quad (10)$$

where $n(=10)$ is the width parameter of the initial cloud droplet spectrum, described by a Gamma function. γ_1 is a tunable constant which determines the efficiency of rain formation and is currently set to 15 in the large-scale parameterization [*Roeckner et al.*, 2003].

[19] The aggregation rate according to *Levkov et al.* [1992] based on work of *Murakami* [1990] is given by:

$$Q_{agg} = \gamma_2 q_{ci} / \Delta t_1 \quad (11)$$

where q_{ci} is the cloud ice mixing ratio in the cloudy part of the grid box ($q_{ci} = q_i/b$), γ_2 is another tunable constant which determines the efficiency of snow formation and is currently set to 95 [*Roeckner et al.*, 2003]. Δt_1 is the time needed for the ice crystal number concentration to decrease from N_i to $N_i(r_{iv}/r_{so})^3$:

$$\Delta t_1 = -\frac{2}{c_l} \log \left(\frac{r_{iv}}{r_{so}} \right)^3 \quad (12)$$

where $r_{so}(=10^{-4} \text{ m})$ is the smallest radius of a particle in the snow class, r_{iv} is the mean volume ice crystal radius and

$$c_l = \frac{q_{ci} \rho a_2 E_{ii} X}{\rho_i} \left(\frac{\rho_0}{\rho} \right)^{0.33} \quad (13)$$

where $a_2(=700 \text{ s}^{-1})$ is an empirical constant, $E_{ii}(=0.1)$ is the collection efficiency between ice crystals, $X(=0.25)$ is the dispersion of the fall velocity spectrum of cloud ice, $\rho_0(=1.3 \text{ kg m}^{-3})$ is the air density at the surface, and $\rho_i(=500 \text{ kg m}^{-3})$ is the density of cloud ice.

[20] The highly nonlinear dependence of these precipitation formation rates on the cloud water and ice content in equation (10) and (11) ensures that the precipitation formed in clouds with little cloud water/ice content is very small, so that the constraint of equation (3) is implicitly included in the new parameterization. In this study, we will conduct the simulations with and without the constraint of equation (3) in the new parameterization to investigate the implication of this constraint.

[21] Accretion of cloud water by raindrops is derived from the stochastic collection equation by *Beheng* [1994]:

$$Q_{ract} = a_3 \rho q_{cl} q_r \quad (14)$$

where q_r is the rainwater mixing ratio and $a_3 = 6 \text{ s}^{-1}$.

[22] Accretion of cloud droplets and ice crystals by snow (riming and collecting ice crystals) is adopted from *Levkov et al.* [1992] based on *Lin et al.* [1983]. Snow crystals are assumed to have an exponent distribution following *Gunn and Marshall* [1958]:

$$n_s(D_s) = n_{0s} \exp(-\lambda_s D_s) \quad (15)$$

where $n_s(D_s)$ is the concentration of particles of diameter D_s per unit size interval. D_s is the diameter of the water drop formed by the melting snow particle. $n_{0s} = 3 \times 10^6 \text{ m}^{-4}$ is the intercept parameter obtained from measurement [*Gunn and Marshall*, 1958]. λ_s is the slope of the particle size distribution and can be described as [*Potter*, 1991]:

$$\lambda_s = \left(\frac{\pi \rho_s n_{0s}}{\rho q_s} \right)^{0.25} \quad (16)$$

where q_s is the snow mixing ratio. $\rho_s = 100 \text{ g m}^{-3}$ is the density of snow.

[23] Collection of supercooled cloud droplets by snow (riming) is based on the geometric sweep-out concept integrated over all snow size for the assumed snow size distribution given in equation (15):

$$Q_{sact} = \gamma_3 \frac{\pi E_{sl} n_{0s} a_4 q_{cl} \Gamma(3 + b_4)}{4 \lambda_s^{3+b_4}} \left(\frac{\rho_0}{\rho} \right)^{0.5} \quad (17)$$

where $a_4 = 4.83$, $b_4 = 0.25$. $E_{sl} = 1$ is the collection efficiency of snow for cloud droplets [*Lin et al.*, 1983]. γ_3 is another tunable factors and is set to 0.1. In the full GCM, γ_1 , γ_2 and γ_3 are tuned by comparing the simulated annual and global mean shortwave and longwave cloud forcing with observations [*Lohmann and Roeckner*, 1996].

[24] The accretion of ice crystals by snow is similar to equation (17):

$$Q_{saci} = \frac{\pi E_{si} n_{0s} a_4 q_{ci} \Gamma(3 + b_4)}{4 \lambda_s^{3+b_4}} \left(\frac{\rho_0}{\rho} \right)^{0.5} \quad (18)$$

where the collection efficiency of snow for cloud ice is assumed to depend on temperature:

$$E_{si} = \exp(0.025(T - T_0)) \quad (19)$$

[25] In the stratiform clouds, accretion of cloud droplets and ice crystals is considered by precipitation falling from the layer above and formed in the same model layer. In the current convective parameterizations, however, accretion of cloud droplets and ice crystals by precipitation falling from the layer above cannot be accounted for because the vertical integration of the mass flux equations starts from the surface as discussed in section 2.1, whereas the integration of the microphysical equations (equations (5) and (6)) in large-scale clouds starts from the cloud top down to the surface. A modification of the vertical integration scheme in convective clouds from upward to downward would be necessary if we tried to take the effect of accretion by falling precipitation into account. It is beyond the scope of the current study. Therefore we only consider the accretion rate of rain/snow with cloud droplets/ice crystals formed in the same model layer. In the large-scale clouds, the accretion rate of rain/snow falling from the layer above has the same order of magnitude as the accretion rate of rain/snow formed in the current layer and is of secondary importance as compared to the autoconversion rate (not shown). However, neglect of the accretion process by rain/snow falling from above certainly can induce larger error in convective clouds due to the importance of this process in convective clouds. This problem will be further addressed in a future study.

[26] Convective cloud cover fraction required for the calculation of the cloud microphysical conversion rates is not diagnosed in the ECHAM5 GCM. Here, we follow the method used in the NCAR Community Climate Model (CCM3) to diagnose the convective cloud fraction as a logarithmic function of the convective mass flux M_u [Kiehl *et al.*, 1996] evaluated by cumulus ensemble model simulations [Xu and Krueger, 1991]

$$b_{conv} = 0.035 \ln(1.0 + M_u) \quad (20)$$

4. Model Simulations

4.1. Forcing and Evaluation Data

[27] As one of the global change research programs, ARM focuses on obtaining field measurements and developing models. Data used in this study are obtained from ARM SGP Intensive Operational Periods (IOPs). Basic observations during IOPs at the ARM site include 3-hourly soundings, surface data from the meteorological network, wind profiler data, radar rainfall and cloud reflectivity from radar and satellite. A description of the ARM SGP clouds and radiation test bed (CART) site with available observa-

tional data, forcing data for SCMs and designs for SCM simulations is given by Ghan *et al.* [2000] and data sets for all the IOPs are available from <http://science.arm.gov/wg/cpm/scm/variational/>. In this study, we will use a subset of the forcing data set generated by the objective analysis method [Zhang and Lin, 1997; Zhang *et al.*, 2001] providing horizontal and vertical temperature and humidity advection and surface fluxes as input for the SCM. We then evaluate the model parameterizations mainly in terms of cloud properties.

[28] Three data sets are used in this study to conduct the simulations: the 1995 summer IOP (18 July to 4 August 1995), the 1997 summer IOP (18 June to 17 July 1997) and the 2002 late spring IOP (25 May to 15 June 2002). The 1995 summer IOP was used as the first effort to conduct a comparison study of SCMs using ARM data [Ghan *et al.*, 2000]. The weather conditions during this IOP were a typical continental summertime regime, ranging from hot, clear days, over local convection to synoptic forcing with precipitation. The 1997 summer IOP can be classified into three weather systems: local convection and frequent, heavy precipitation; clear and hot days; and a large, convective complex with sustained precipitation. This IOP has been chosen for another intercomparison of SCMs and cloud-resolving models (CRMs) conducted jointly by ARM and the GEWEX Cloud System Study (GCSS) [Xie *et al.*, 2002; Xu *et al.*, 2002]. The aim of the 2002 spring IOP is to understand initiation of convection and to test the convective cumulus parameterizations in SCMs and associated GCMs.

4.2. SCM Simulation and Discussion

[29] The SCM we used in this study has 19 vertical levels and a time step of 30 minutes. The forcing data to drive the SCM simulation are 3-hourly horizontal and vertical advective tendencies of temperature and moisture, observed surface sensible and latent heat fluxes and surface temperature specified from observations as described in the work of Ghan *et al.* [2000] for the SCM intercomparison study using the 1995 summer ARM SGP IOP data. The forcing data are linearly interpolated and applied to every model time step (30 minutes). Vertical forcing data, such as temperature and moisture advection are also linearly interpolated to the vertical resolution of the SCM.

[30] In this study, three model setups are examined. ORIG represents the standard ECHAM5 model setup. CONV-A is a model setup with the new microphysical parameterization for convective clouds. In CONV-A, convective precipitation is allowed to form at all levels of the convective clouds which is different from the standard ECHAM5, in which precipitation is suppressed at low levels of convective clouds as defined in equation (3). CONV-P is the same as CONV-A, but precipitation is prohibited at low levels of the convective clouds for the same Δp_{crit} range above cloud base as applied in ORIG.

4.2.1. Temperature and Specific Humidity

[31] Temperature and specific humidity are the main fields that determine cloud formation. Figures 1 and 2 show the SCM simulated mean profiles of temperature and specific humidity biases from observations. In Figure 1, a noticeable cold bias as large as 5 K around 400 hPa is revealed for all three model setups, and dry biases below

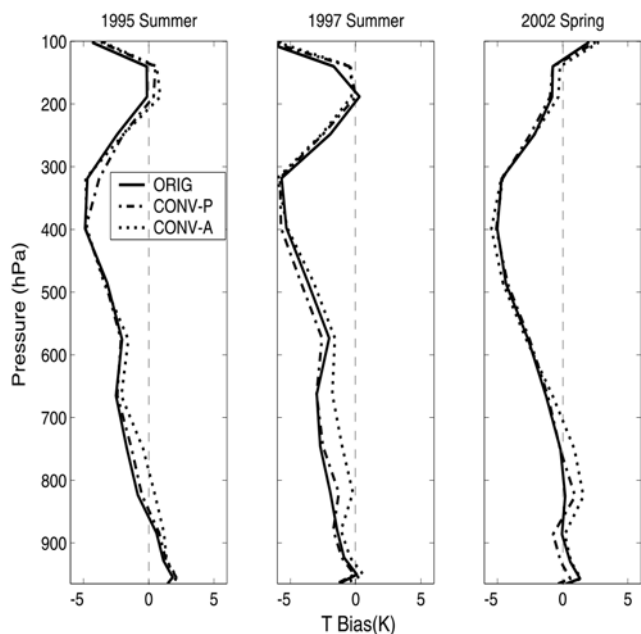


Figure 1. IOP averaged profiles of the temperature bias for the simulations.

800 hPa are shown in Figure 2. Temperature and moisture tendency biases in the forcing data may be one reason that causes the departure of model simulated temperature and moisture from observations. Lack of parameterization of cloud dynamics that can account for mesoscale updrafts and downdrafts in the model can also be a reason. Below 600 hPa, the temperature simulated in the CONV-A setup tends to be warmer than simulated in the ORIG and CONV-P setups. The atmosphere is drier between 500 hPa and 800 hPa using the new parameterization than using the

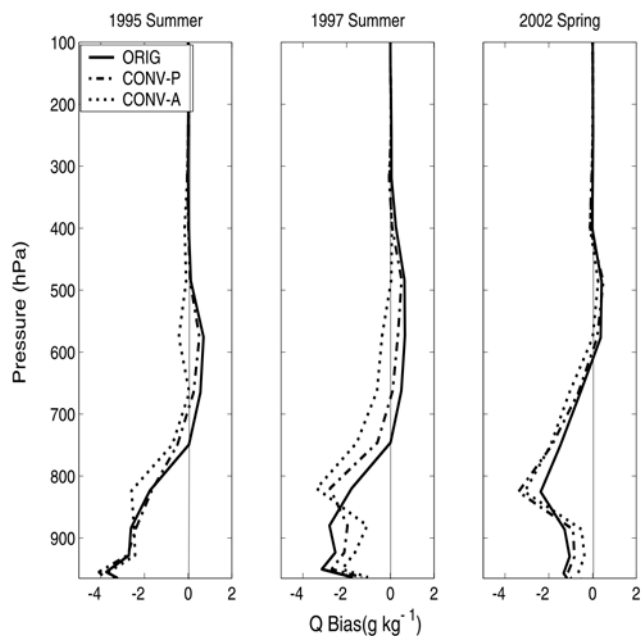


Figure 2. IOP averaged profiles of the humidity bias for the simulations.

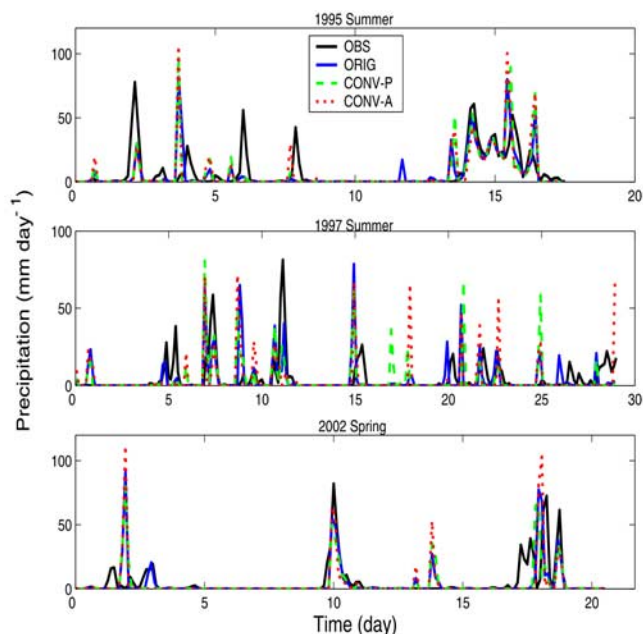


Figure 3. Comparison of the three hourly mean precipitation.

original parameterization. Near the surface, the differences in temperature among these three setups decrease, and the atmosphere is wetter using the new parameterization than using the original one for the 1997 summer and 2002 spring IOPs. The assumption that precipitation can form at all levels in the convective clouds in the CONV-A setup is the reason for the warmest and driest condition simulated by CONV-A between 500 hPa and 800 hPa because precipitation is removed from the atmosphere once it has been formed at low levels of the clouds. Therefore the atmosphere becomes drier and the latent heat released during the precipitation formation warms the atmosphere. The wetter conditions simulated by CONV-A near the surface during the 1997 summer and 2002 spring IOPs are caused by evaporation of cloud water and precipitation, vertical diffusion and less condensation of water vapor.

4.2.2. Precipitation, Liquid Water Path, and Ice Water Path

[32] Precipitation, liquid water path (LWP) and ice water path (IWP) are the fields most closely related to the cloud microphysical parameterizations. Figures 3 and 4 show the comparison of 3-hourly mean surface precipitation and accumulated precipitation during the simulated periods. The correlation coefficients between the model simulations and the observations are summarized in Table 1, and Table 2 compares the IOP averaged values and RMS (Root Mean Square) differences.

[33] Model simulations slightly underestimate the accumulated precipitation as shown in Figure 4 and Table 2. SCM simulations capture almost all the major precipitation events with some spurious events during nonprecipitation periods, such as around days 9 and 18 of the 1997 summer IOP and around day 14 during the 2002 spring IOP as shown in Figure 3. The spurious events were also found in several model simulations compiled by *Xie et al.* [2002]

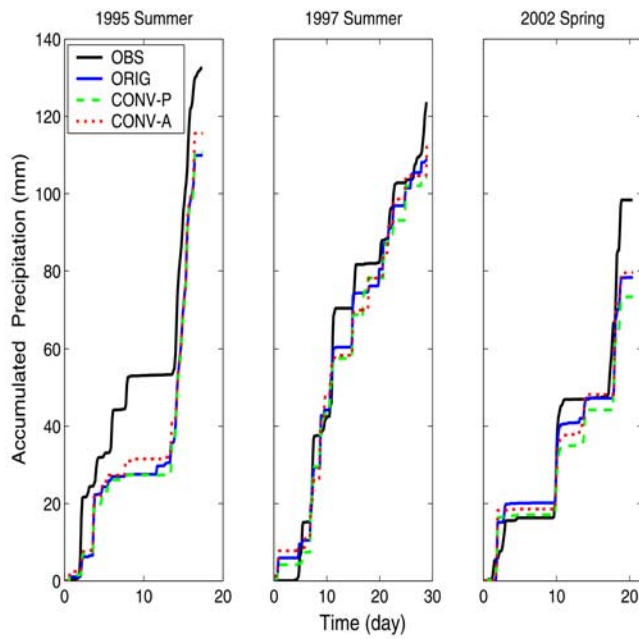


Figure 4. Comparison of the accumulated precipitation.

when they compared a large number of SCMs during the 1997 summer IOP. These spurious precipitation events may be related to the different triggering mechanisms for convection as discussed by *Xie et al.* [2002].

[34] Because in the CONV-A setup precipitation is allowed to form and fall to the surface from all levels of the clouds as shown in Figure 5, it generally produces slightly more precipitation than the other two model setups

Table 1. Correlation Coefficients Between Simulated and Observed Values of Precipitation, Liquid Water Path (LWP), Total Cloud Cover (TCC), Outgoing Longwave Radiation (OLR), and Net Downward Solar Radiation at the Top of the Atmosphere (F_{top}^{sw}) for the Different Model Simulations Based on 3-Hourly Values

	ORIG	CONV-P	CONV-A
<i>Precipitation</i>			
1995 summer	0.50	0.45	0.39
1997 summer	0.24	0.19	0.11
2002 spring	0.38	0.39	0.25
<i>LWP</i>			
1995 summer	0.47	0.28	0.59
1997 summer	0.42	0.43	0.47
2002 spring	0.57	0.40	0.41
<i>TCC</i>			
1995 summer	0.50	0.55	0.56
1997 summer	0.33	0.46	0.33
2002 spring	0.43	0.33	0.33
<i>OLR</i>			
1995 summer	0.67	0.67	0.67
1997 summer	0.48	0.52	0.44
2002 spring	0.64	0.58	0.59
F_{top}^{sw}			
1995 summer	0.90	0.91	0.91
1997 summer	0.87	0.86	0.88
2002 spring	0.91	0.91	0.91

Table 2. Comparison of IOP Averaged Values Between the Different Model Simulations With Observations and RMS Differences for Different Model Simulations Based on 3-Hourly Data

	OBS Mean	ORIG		CONV-P		CONV-A	
		Mean	RMS	Mean	RMS	Mean	RMS
<i>Precipitation, mm/day</i>							
1995 summer	7.57	6.28	14.6	6.33	16.4	6.60	17.4
1997 summer	4.26	3.76	13.0	3.60	13.6	3.91	15.2
2002 spring	4.80	3.82	14.6	3.57	13.9	3.88	17.7
<i>LWP, g m⁻²</i>							
1995 summer	21.1	87.4	140.8	127.4	224.7	46.9	91.4
1997 summer	29.7	47.8	90.6	110.3	177.6	25.0	59.2
2002 spring	45.0	34.9	69.8	80.6	139.0	25.4	76.4
<i>IWP, g m⁻²</i>							
1995 summer		44.6		39.3		35.2	
1997 summer		30.8		24.4		23.5	
2002 spring		26.3		22.5		23.3	
<i>TCC, %</i>							
1995 summer	55.1	66.3	40.7	58.7	38.7	54.7	38.1
1997 summer	42.8	76.4	51.3	68.4	46.1	64.2	47.0
2002 spring	42.7	56.8	45.4	65.6	51.0	57.4	48.7
<i>OLR, W m⁻²</i>							
1995 summer	251.8	211.8	59.5	219.4	55.8	228.7	51.9
1997 summer	262.2	213.1	65.6	224.0	59.5	233.8	57.6
2002 spring	253.7	231.6	49.2	229.6	50.3	235.8	49.0
$F_{top}^{sw}, W m^{-2}$							
1995 summer	305.6	292.7	141.1	310.3	129.2	326.8	113.5
1997 summer	363.9	316.7	113.2	318.9	118.3	343.7	84.4
2002 spring	345.4	325.0	82.7	303.7	110.4	327.6	86.4

as shown in Figure 4 and Table 2. If we analyze individual precipitation events, CONV-A, however, sometimes simulates less precipitation because precipitation produced at the lower cloud level can reduce the subsequent vertical development of the clouds and thus transport less moisture to the upper levels and generate less precipitation in the upper levels (Figure 5). The results in Table 1 show that the model simulated 3-hourly mean precipitation correlates well with the observations (above 99% confidence level) except for the 1997 summer IOP (above 95% confidence level) where frequent precipitation occurred. This may be caused by the convection trigger mechanism as mentioned above. However, the simulated accumulated precipitation follows the trend in the observations well as shown in Figure 4.

[35] Figure 6 shows the comparison of SCM simulated 3-hourly mean LWP with the observed LWP by Microwave Radiometer (MWR) [*Liljegren and Lesht, 1996*]. The model simulations and observations have a good correlation as shown in Table 1 (above 99% confidence level) although the observed LWP is a point value while the model simulation is a grid box average. LWP is drastically overestimated in the CONV-P setup for all three IOPs as shown in Figure 6 and Table 2. The ORIG and CONV-A setups produce reasonable amounts of LWP for the 1997 summer and 2002 spring IOPs. During the 1995 summer IOP, all 3 setups overestimate LWP with CONV-A producing the smallest amount (see Table 2 for details) and agreeing best with observations. CONV-A simulates the smallest LWP because clouds at the lower levels consist of more liquid

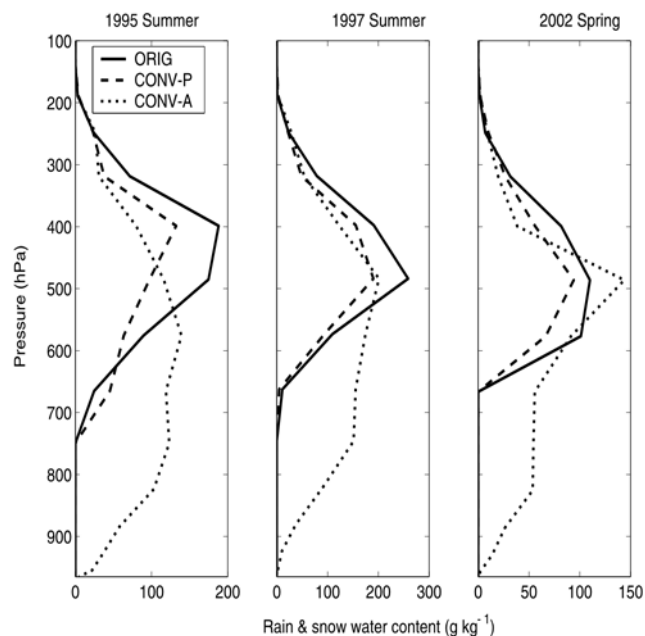


Figure 5. Comparison of profiles for rain plus snow water content formed in the convective cloud formation.

water than at higher levels. If the precipitation can form at each level in the clouds as assumed in CONV-A, part of the liquid water in the lower layers of the clouds is converted into precipitation, thus CONV-A simulates the smallest LWP. Although ORIG and CONV-P both suppress the formation of precipitation in the lower levels of the clouds, their precipitation formation parameterizations are very different. In ORIG, the conversion rate of precipitation is the same regardless of the cloud phase and cloud water content (equation (2)), whereas the formation of precipitation in CONV-P is parameterized by equation (10) for the

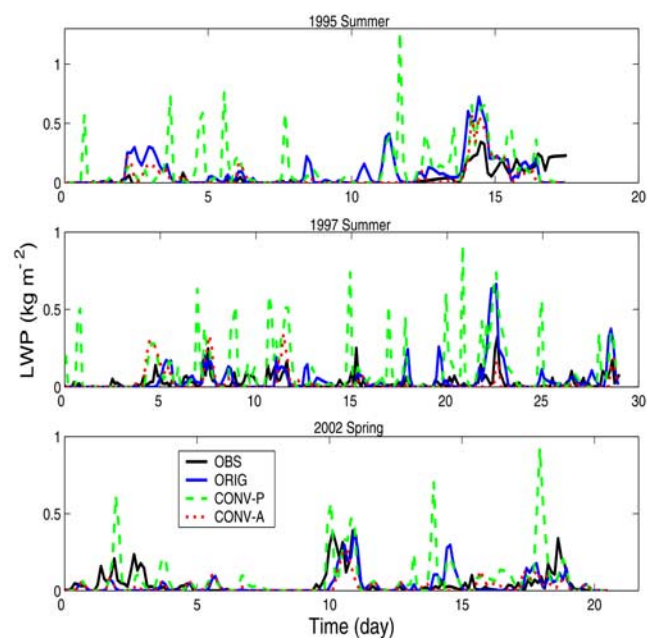


Figure 6. Comparison of the three hourly mean LWP.

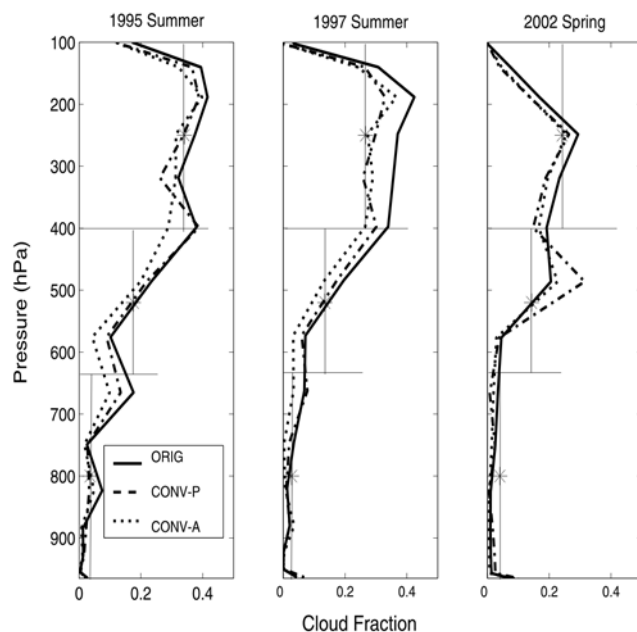


Figure 7. IOP averaged profiles of cloud cover fraction. Stars represent the low, midlevel, and high cloud cover fraction observed by GOES satellite.

autoconversion of liquid water, equation (11) for the aggregation of cloud ice and the accretions processes by equations (14), (17) and (18). Generally, the precipitation formed by liquid water processes is less than that formed via the ice phase so that more liquid water is left in the cloud in CONV-P than in ORIG.

[36] The model simulated ice water path (IWP) averaged over the different IOPs is also listed in Table 2. Although there are large differences in LWPs, IWP exhibits only small differences, because the precipitation formation via the ice phase is generally more efficient than via the liquid phase [Rogers and Yau, 1989]. This means that the new microphysical parameterization mainly influences the warm cloud processes.

4.2.3. Large-Scale Cloud Fraction

[37] In ECHAM5, the PDF based cloud cover scheme [Tompkins, 2002] can represent the growth and decay of cirrus cloud decks and the creation of cloud in clear sky or breakup of an overcast cloud deck due to boundary layer turbulence. Vertical mean profiles of large-scale cloud fraction are shown in Figure 7. The stars in the figure are the averages of GOES satellite observed low ($p > 631$ hPa), midlevel ($400 \text{ hPa} < p < 631$ hPa) and high ($p < 400$ hPa) cloud fraction during these periods. We can see that the model simulated cloud fractions agree well with the satellite observations. The maximum cloud cover occurs at an altitude around 300 hPa with a mean cloud fraction of about 35% indicating that convection induced high clouds dominate in this region. CONV-A produces less cloud cover below 400 hPa than ORIG and CONV-P. This is consistent with the precipitation simulations, such that more precipitation is produced, less moisture remains and fewer clouds form in CONV-A. Generally, the time averaged total cloud cover simulated by CONV-A agrees best with observation (Table 2).

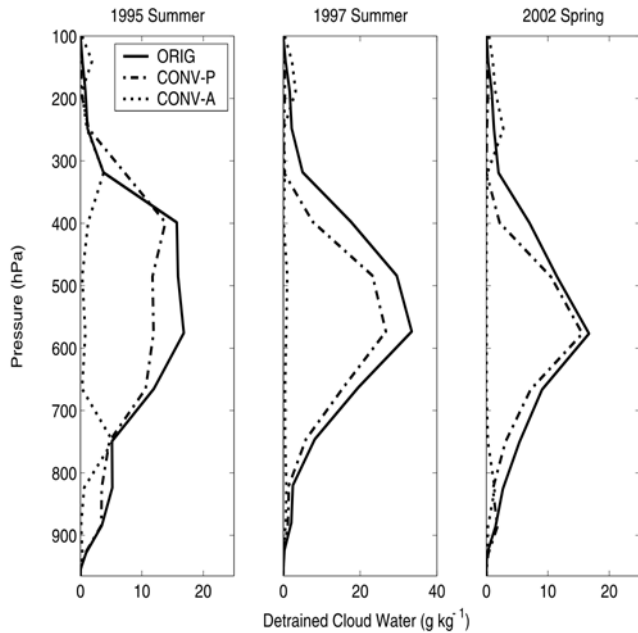


Figure 8. IOP averaged profiles of detrained cloud water (liquid plus ice). Note that the detrained cloud water in setup CONV-A is multiplied by a factor of 10.

4.2.4. Detrained Cloud Water From Convective Clouds

[38] Detrainment of moisture and cloud water to the environment is the primary process through which convective cloud systems influence the large-scale moisture budget. Figure 8 shows the profiles of total detrained cloud water content. The ORIG and CONV-P setups produce similar amounts of detrained cloud water with a maximum around 600 hPa, while the maximum in CONV-A setup is around 200 to 300 hPa, which agrees best with the obser-

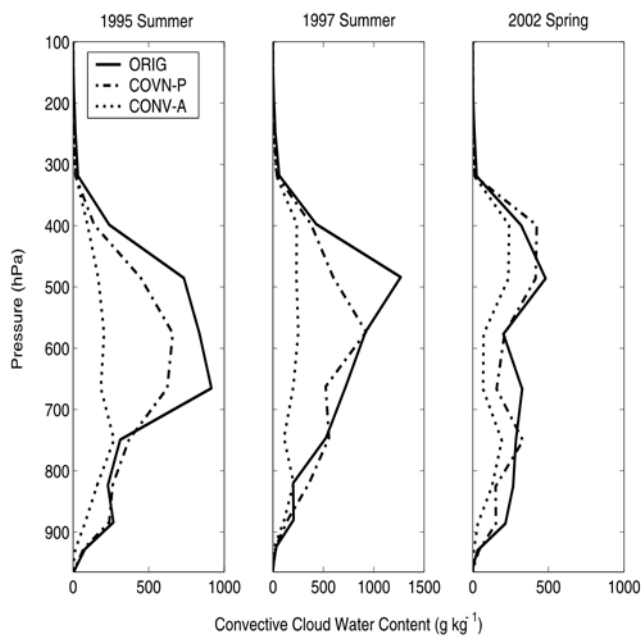


Figure 9. IOP averaged profiles of convective cloud water content (liquid plus ice).

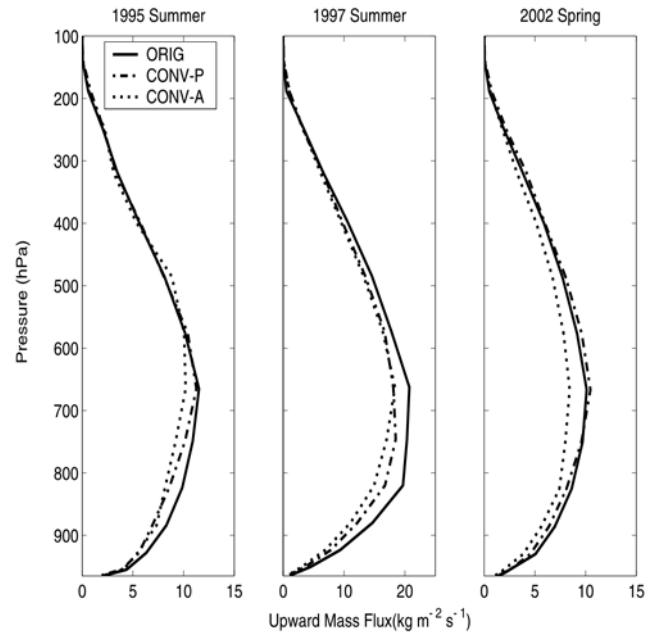


Figure 10. IOP averaged profiles of upward mass flux.

vational results for deep convective clouds over continents in midlatitudes [Cotton and Anthes, 1989]. Because the difference between CONV-A and CONV-P is only the precipitation formation assumption in lower level of convective clouds, the large difference in detrained cloud water is caused by the subsequent cloud development at higher levels of the convective clouds. The detrained cloud water amount is determined by the term $D_u l$ in equation (1). D_u includes turbulent detrainment and organized outflow at cloud top and is proportional to the upward mass flux M_u [Tiedtke, 1989]. Figure 9 shows the model simulated cloud water content in convective clouds. We can see that the cloud water content simulated by CONV-A is smaller than in the other two setups because more precipitation is formed. M_u in CONV-A is also slightly smaller than in ORIG and CONV-P as shown in Figure 10. Hence the detrained water content is the smallest in CONV-A.

4.2.5. Radiation

[39] The main goal of extending the microphysical parameterization to convective cloud is to simulate aerosol effects on clouds more realistically in climate models. Thus it is interesting to evaluate the effect of the new parameterization on the radiation fields. Comparisons of two parameters are shown here, one is outgoing longwave radiation (OLR) and another one is net downward radiation at the top of the atmosphere (F_{top}^{sw}). The correlation coefficients between the model simulations and observations are summarized in Table 1, and comparisons of the IOP averaged radiative fluxes are listed in Table 2.

[40] The SCM simulated OLR correlates well (above 99% confidence) with the observed as shown in Table 1. However, the SCM significantly underestimates OLR in all simulations (Table 2). With the original model setup, OLR is underestimated by as much as 40 W m^{-2} in the 1995 and 1997 summer IOPs. The new microphysical parameterization improves the SCM simulation significantly,

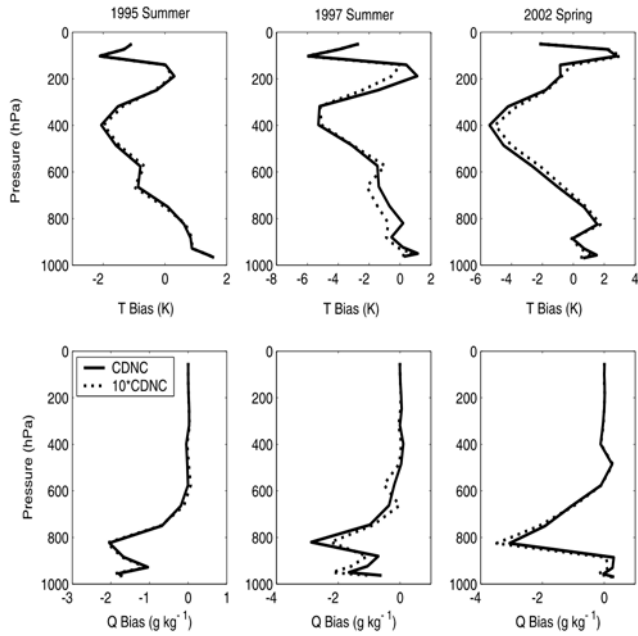


Figure 11. Influence of the increased cloud droplet number concentration (CDNC) on the simulated temperature and humidity fields.

especially for CONV-A, which produces a higher OLR by $15\text{--}20\text{ W m}^{-2}$ due to its smallest water content and cloud cover and thus agrees better with observations than ORIG in the 1995 and 1997 summer IOPs.

[41] Because of the diurnal cycle of shortwave radiation, the model simulated net downward radiations at the top of the atmosphere (F_{top}^{sw}) correlates very well with observation

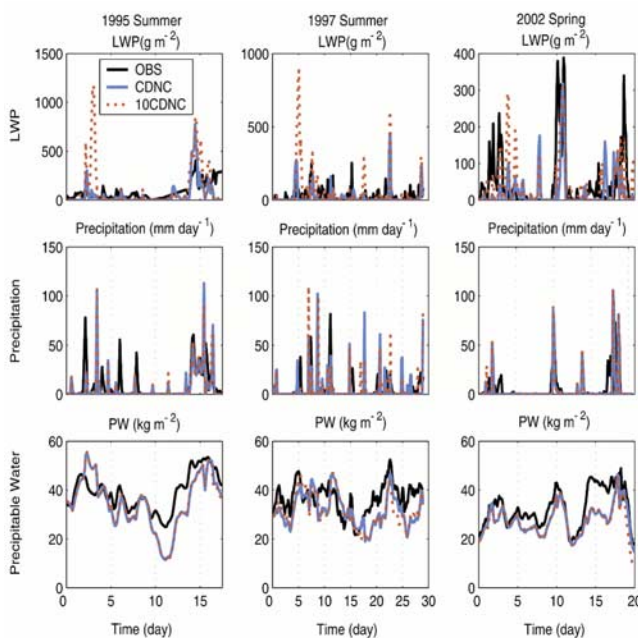


Figure 12. Influence of the increased cloud droplet number concentration (CDNC) in CONV-A setup on the simulated precipitation, LWP, and precipitable water as compared with observation.

Table 3. Comparison of IOP Averaged Values Between the Different Model Simulations With Observations for CONV-A Model Setup With Different CDNC

	OBS	CONV-A	CONV-A $10 \times$ CDNC
<i>LWP, g m⁻²</i>			
1995 summer	21.1	53.0	105.7
1997 summer	29.7	17.4	54.0
2002 spring	45.0	23.3	37.4
<i>Precipitation, mm/day</i>			
1995 summer	7.57	6.17	6.43
1997 summer	4.26	4.08	3.93
2002 spring	4.80	4.18	4.37
<i>PW, kg m⁻²</i>			
1995 summer	39.2	34.9	35.0
1997 summer	36.5	32.1	31.9
2002 spring	32.4	27.7	27.3
<i>IWP, g m⁻²</i>			
1995 summer		35.7	36.4
1997 summer		23.4	22.9
2002 spring		19.1	18.9
<i>TCC, %</i>			
1995 summer	55.1	56.8	59.8
1997 summer	42.8	66.8	64.1
2002 spring	42.7	47.8	51.2
<i>OLR, W m⁻²</i>			
1995 summer	251.8	228.0	227.1
1997 summer	262.2	230.6	234.0
2002 spring	253.7	244.1	245.1
<i>F_{top}^{sw}, W m⁻²</i>			
1995 summer	305.6	327.0	324.7
1997 summer	363.9	343.6	338.6
2002 spring	345.4	338.9	331.8

based on 3-hourly values (Table 1). As shown in Table 2, ORIG underestimates F_{top}^{sw} in all three setups, especially in the 1997 summer IOP where the underestimation amounts to 47 W m^{-2} . The highest F_{top}^{sw} is simulated by the CONV-A setup again due to its smaller water content and cloud cover and agrees best with observations for the 1997 and 2002 summer IOPs.

4.3. Sensitivity Study on Cloud Droplet Number Concentration

[42] Many studies have addressed the aerosol indirect effect on climate, which, however, is mainly evaluated for stratiform clouds because microphysical parameterizations for convective clouds used in climate models are very simple. In this section, we will investigate the sensitivity of the model simulation to CDNC in both stratiform and convective clouds by increasing CDNC by a factor of 10.

[43] In section 4.2, we used observed surface sensible and latent fluxes in conducting SCM simulations as suggested by ARM SCM intercomparison projects [Ghan *et al.*, 2000; Xie *et al.*, 2002]. However, changes in CDNC will affect the surface fluxes. Therefore the model simulated surface fluxes are used for the sensitivity studies. All three IOPs are chosen for these sensitivity studies using the CONV-A model setup because CONV-A generally performs better than CONV-P.

[44] As shown in Figure 11, the increase in CDNC can change the temperature and humidity by up to 1 K

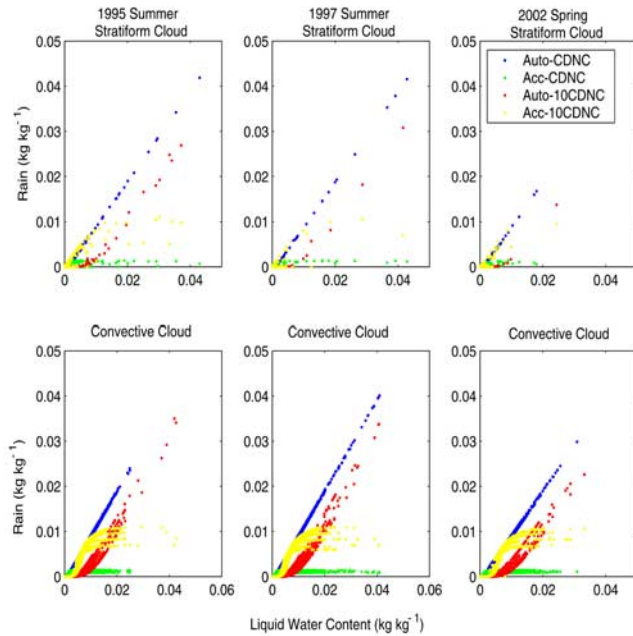


Figure 13. Change of conversion of liquid water content to rain through the autoconversion and accretion processes in two CDNC scenarios.

and 2 g kg^{-1} , respectively. The influence of increased CDNC on the precipitation, LWP and precipitable water (PW) during all the IOPs is shown in Figure 12 and IOP averaged values are compared in Table 3. Larger LWPs are produced for all IOPs when CDNC is increased, which is the result of the inverse relationship of CDNC and the autoconversion rate as described in equation (10). When CDNC is increased ten-fold, the IOP averaged LWPs are increased by about 100%, 200% and 50% for 1995 summer, 1997 summer and 2002 spring IOP, respectively. However, the increase in CDNC hardly changes the IWP as shown in Table 3.

[45] Although LWP and individual precipitation events change substantially as shown in Figure 12, the average amount of precipitation only change slightly (Table 3). The reason is that, on the one hand, the change in precipitation at one time step will change the hydrological cycle in the atmosphere, which consequently changes the subsequent precipitation formation. On the other hand, the decrease in the autoconversion rate due to the increase in CDNC results in a higher cloud liquid water content, which leads to higher accretion rates (equations (14) and (17)) as shown in Figure 13. It shows that precipitation is mainly produced by convective clouds during these IOPs and that the decrease in precipitation due to the reduced autoconversion rates has a similar magnitude as the increase in precipitation by the higher accretion rates, so that the increase in CDNC does not necessarily result in decreasing precipitation. On the contrary, simulations of two of the three IOPs show that increases in CDNC slightly enhances precipitation, which agrees with other cloud-resolving and mesoscale model simulations [Tao *et al.*, 2004; Khain *et al.*, 2005; Lohmann *et al.*, 2003]. However, a 10-fold increase in CDNC does not lead to an increase in precipitation if the observed sensible and latent heat fluxes are used to force the SCM (results are not shown). Thus the feedback between soil

moisture and precipitation may be responsible for that [Koster *et al.*, 2004]. This will be investigated further in future.

[46] From Table 3, we can see that the SCM simulates less precipitation than observed. Meanwhile, it simulated drier condition than observed as indicated by the comparison of IOP averaged precipitable water. This phenomenon also occurs when comparing different SCM simulations. For instance, the SCM simulated slightly less precipitation for the 1997 summer IOP with a 10-fold increase of CDNC, the simulated precipitable water, however, is also smaller than simulated with the original CDNC. The reason for this apparent contradiction is that precipitation events occur at different times and with different precipitation rates in the observations and in the SCM simulations as illustrated in Figure 12. For example, during the 1997 summer IOP, the SCM simulates a spurious precipitation event in the beginning of the IOP, which decreases the SCM simulated precipitable water. Since the humidity field in SCM is forced by the observed moisture advection, the simulated precipitable water remains smaller than observed until the first observed precipitation event near day 6. After that, the SCM simulated precipitable water varies depending on whether the SCM simulated precipitation rate is larger or smaller than observed. Near day 11, the SCM simulates a smaller precipitation event than observed leading to larger simulated precipitable water than observed afterward until next precipitation event occurs near day 15. Another large spurious precipitation event right after day 17 causes the SCM simulated precipitable water to remain smaller than observed until the end of this IOP. Therefore the SCM simulated IOP average precipitable water can be smaller than observed although less precipitation is simulated.

[47] The effect of increasing CDNC on cloud cover fraction is summarized in Table 3. Total cloud cover may decrease by 2.7% as shown during the 1997 summer IOP or increase by 3.0 to 3.4% as during the 1995 summer and 2002 spring IOP. Influences of increasing CDNC on OLR and net downward radiation at the top of the atmosphere (F_{top}^{sw}) are also summarized in Table 3. Larger CDNC causes a decrease in F_{top}^{sw} despite the increase or decrease in total cloud cover.

5. Conclusions

[48] Cloud properties observed during two summer and one late spring IOPs at the ARM SGP site in Oklahoma are simulated with the ECHAM5 SCM to evaluate a microphysical parameterization in simulating convective clouds over midlatitude continents. Results show that the SCM is generally able to reproduce the observed microphysical properties. One reason for the good performance of the model to simulate precipitation is that the boundary conditions are constrained by observation. The new parameterization performs at least as well as the original model setup in terms of simulating cloud properties and precipitation. A clear improvement is seen in the simulation of radiation.

[49] Sensitivity studies show that a higher LWP is simulated when CDNC is increased due to the decrease of the autoconversion rate. Meanwhile, a higher accretion rate is simulated in the higher CDNC scenario because more liquid water is retained in the clouds. Therefore in contrary to the

expected decrease the precipitation, the simulated total precipitation increases slightly for two of the three IOPs agreeing with the results simulated in cloud-resolving and mesoscale models [Tao et al., 2004; Khain et al., 2005; Lohmann et al., 2003].

[50] With this new parameterization, aerosol effects on both stratiform and convective clouds can be studied in climate models to reveal a more realistic estimate of aerosol effects on climate. However, we focused only on investigating the new parameterization for the simulation of midlatitude continental convective cloud systems in this study. Research on how well the parameterization performs in simulating convective clouds in other climatic region, such as the tropics, and how well it performs in the global model will be evaluated in future studies. Even though this scheme represents a step toward a more realistic simulation of convection in the GCM, much more needs to be done. For instance, mesoscale updraft and downdraft should be included, accretion of rain and snow falling into the cloud deck from above and adding a graupel category as an ice phase of convective precipitation need to be considered, and slanted convection may be important as well.

[51] **Acknowledgments.** This study is supported by the Modeling of Clouds and Climate (MOC2) project funded by the National Science and Research Council of Canada (NSERC), the Canadian Foundation for Climate and Atmospheric Science (CFCAS), and the Meteorological Service of Canada (MSC). Authors thank the Atmospheric Radiation Measurement Program (ARM) funded by U.S. Department of Energy for providing the forcing and observational data. We also highly appreciate the useful comments from Daniel Rosenfeld and the two anonymous reviewers.

References

- Ackerman, A. S., O. B. Toon, D. E. Stevens, A. J. Heymsfield, V. Ramanathan, and E. J. Welton (2000), Reduction of tropical cloudiness by soot, *Science*, **288**, 1042–1047.
- Andreae, M. O., D. Rosenfeld, P. Artaxo, A. A. Costa, G. P. Frank, K. M. Longo, and M. A. F. Silva-Dias (2004), Smoking rain clouds over the Amazon, *Science*, **303**, 1337–1342.
- Beheng, K. D. (1994), A parameterization of warm cloud microphysical conversion processes, *Atmos. Res.*, **33**, 193–206.
- Bigg, E. K. (1953), The supercooling of water, *Proc. Phys. Soc.*, **66**, 688–694.
- Boudala, F. S., G. A. Isaac, S. G. Cober, Q. Fu, and A. V. Korolev (2002), Parameterization of liquid fraction in terms of temperature and cloud water content in stratiform mixed phase clouds, paper presented at 11th Conference on Cloud Physics, Am. Meteorol. Soc., Ogden, Utah.
- Cotton, W. R., and R. A. Anthes (1989), Storm and cloud dynamics, pp. 237–243, Elsevier, New York.
- Deutsches Klimarechenzentrum (DKRZ) (1993), The ECHAM3 atmospheric general circulation model, *Rep. 6*, Modellbetreuungsgruppe, Hamburg, Germany.
- Foster, D. S. (1958), Thunderstorm gusts compared with computed downdraft speeds, *Mon. Weather Rev.*, **86**, 91–94.
- Fritsch, J. M., and C. G. Chappell (1980), Numerical prediction of convectively driven mesoscale pressure systems, part I: Convective parameterization, *J. Atmos. Sci.*, **37**, 1722–1733.
- Ghan, S., et al. (2000), A comparison of single column model simulations of summertime midlatitude continental convection, *J. Geophys. Res.*, **105**, 2091–2124.
- Grabowski, W. W. (2003), Impact of cloud microphysics on convective-radiative quasi equilibrium revealed by cloud-resolving convection parameterization, *J. Clim.*, **16**, 3463–3475.
- Gunn, K. L. S., and J. S. Marshall (1958), The distribution with size of aggregate snowflakes, *J. Meteorol.*, **15**, 452–461.
- Hobbs, P. V., J. S. Reid, R. A. Kotchenruther, R. J. Ferek, and R. Weiss (1997), Direct radiative forcing by smoke from biomass burning, *Science*, **275**, 1776–1778.
- Khain, A. P., D. Rosenfeld, and A. Pokrovsky (2001), Simulating convective clouds with sustained supercooled liquid water down to -37.5°C using a spectral microphysics model, *Geophys. Res. Lett.*, **28**, 3887–3890.
- Khain, A. P., D. Rosenfeld, and A. Pokrovsky (2005), Aerosol impact on the dynamics and microphysics of convective clouds, *Q. J. R. Meteorol. Soc.*, in press.
- Kiehl, J. T., J. J. Hack, G. B. Bonan, B. A. Boville, B. P. Briegleb, D. L. Williamson, and P. J. Rasch (1996), Description of the NCAR Community Climate Model (CCM3), *NCAR Tech. Note TN-420+STR*, Natl. Cent. for Atmos. Res., Boulder, Colo.
- Koster, R. D., et al. (2004), Regions of strong coupling between soil moisture and precipitation, *Science*, **305**, 1138–1140.
- Levkov, L., B. Rockel, H. Kapitzka, and E. Raschke (1992), 3D mesoscale numerical studies of cirrus and stratus clouds by their time and space evolution, *Beitr. Phys. Atmos.*, **65**, 35–58.
- Liljegren, J. C., and B. M. Lesht (1996), Measurements of integrated water vapor and cloud liquid water from microwave radiometers at the DOE ARM cloud and radiation testbed in the U. S. Southern Great Plains, paper presented at IEEE International Geosciences and Remote Sensing Symposium, Inst. of Electr. and Electron. Eng., Lincoln, Neb.
- Lin, Y. L., R. D. Farley, and H. D. Orville (1983), Bulk parameterization of the snow field in a cloud model, *J. Clim. Appl. Meteorol.*, **22**, 1065–1092.
- Lohmann, U., and J. Feichter (1997), Impact of sulfate aerosols on albedo and lifetime of clouds: A sensitivity study with the ECHAM4 GCM, *J. Geophys. Res.*, **102**, 13,685–13,700.
- Lohmann, U., and E. Roeckner (1996), Design and performance of a new cloud microphysical scheme developed for the ECHAM general circulation model, *Clim. Dyn.*, **12**, 557–572.
- Lohmann, U., J. Feichter, J. E. Penner, and R. Leaitch (2000), Indirect effects of sulfate and carbonaceous aerosols: A mechanistic treatment, *J. Geophys. Res.*, **105**, 12,193–12,206.
- Lohmann, U., J. Zhang, and J. Pi (2003), Sensitivity studies of the effect of increased aerosol concentrations and snow crystal shape on the snowfall rate in the Arctic, *J. Geophys. Res.*, **108**(D11), 4341, doi:10.1029/2003JD003377.
- Murakami, M. (1990), Numerical modeling of dynamical and microphysical evolution of an isolated convective cloud—The 19 July 1981 CCOPE cloud, *J. Meteorol. Soc. Jpn.*, **68**, 107–128.
- Nober, F. J., H.-F. Graf, and D. Rosenfeld (2003), Sensitivity of the global circulation to the suppression of precipitation by anthropogenic aerosols, *Global Planet. Change*, **37**, 57–80.
- Nordeng, T. (1994), Extended versions of the convective parameterization scheme at ECMWF and their impact on the mean and transient activity of the model in the tropics, *Tech. Memo. 206*, Eur. Cent. for Med. Range Weather Forecast., Reading, UK.
- Peng, Y., and U. Lohmann (2003), Sensitivity study of the spectral dispersion of the cloud droplet size distribution on the indirect aerosol effect, *Geophys. Res. Lett.*, **30**(10), 1507, doi:10.1029/2003GL017192.
- Penner, J. E., C. C. Chuang, and K. Grant (1998), Climate forcing by carbonaceous and sulfate aerosols, *Clim. Dyn.*, **14**, 839–851.
- Potter, B. E. (1991), Improvements to a commonly used cloud microphysical bulk parameterization, *J. Appl. Meteorol.*, **30**, 1040–1042.
- Ramaswamy, V., et al. (2001), Radiative forcing of climate change, in *Climate Change 2001: The Scientific Basis*, chap. 6, pp. 375–379, Cambridge Univ. Press, New York.
- Roeckner, E., et al. (2003), The atmospheric general circulation model ECHAM 5. Part I: Model description, *MPI Rep. 349*, Max Planck Inst. for Meteorol., Hamburg.
- Roelofs, G. J., J. Lelieveld, and L. Ganzeveld (1998), Simulation of global sulfate distribution and the influence on effective cloud drop radii with a coupled photochemistry sulfur cycle model, *Tellus, Ser. B*, **50**, 224–242.
- Rogers, R. R., and M. K. Yau (1989), *A Short Course in Cloud Physics*, Elsevier, New York.
- Rosenfeld, D. (1999), TRMM observed first direct evidence of smoke from forest fires inhibiting rainfall, *Geophys. Res. Lett.*, **26**, 3105–3108.
- Rosenfeld, D. (2000), Suppression of rain and snow by urban and industrial air pollution, *Science*, **287**, 1793–1796.
- Rosenfeld, D., and I. M. Lensky (1998), Satellite-based insights into precipitation formation processes in continental and maritime convective clouds, *Bull. Am. Meteorol. Soc.*, **79**, 2457–2476.
- Rotstayn, L. D., B. F. Ryan, and J. E. Penner (1996), Precipitation changes in a GCM resulting from the indirect effects of anthropogenic aerosols, *Geophys. Res. Lett.*, **27**, 3045–3048.
- Tao, W.-K., X. Li, A. Khain, J. Simpson, D. Johnson, and L. Remer (2004), The impact of aerosols on cloud and precipitation processes: Cloud-resolving model simulations, paper presented at 14th International Conference on Clouds and Precipitation, Int. Comm. on Clouds and Precip. (ICCP), Bologna, Italy.
- Tiedtke, M. (1989), A comprehensive mass flux scheme for cumulus parameterization in large-scale models, *Mon. Weather Rev.*, **117**, 1779–1800.
- Tiedtke, M. (1993), Representation of clouds in large-scale models, *Mon. Weather Rev.*, **121**, 3040–3061.

- Tompkins, A. M. (2002), A prognostic parameterization for the subgrid-scale variability of water vapor and clouds in large-scale models and its use to diagnose cloud cover, *J. Atmos. Sci.*, *59*, 1917–1942.
- Xie, S. C., et al. (2002), Intercomparison and evaluation of cumulus parameterizations under summertime midlatitude continental conditions, *Q. J. R. Meteorol. Soc.*, *128*, 1095–1135.
- Xu, K.-M., and S. K. Krueger (1991), Evaluation of cloudiness parameterizations using a cumulus ensemble model, *Mon. Weather Rev.*, *119*, 342–367.
- Xu, K.-M., et al. (2002), An intercomparison of cloud-resolving models with the atmospheric radiation measurement summer 1997 intensive observation period data, *Q. J. R. Meteorol. Soc.*, *128*, 593–624.
- Zhang, M. H., and J. L. Lin (1997), Constrained variational analysis of sounding data based on column-integrated budgets of mass, heat, moisture, and momentum: Approach and application to ARM measurements, *J. Atmos. Sci.*, *54*, 1503–1524.
- Zhang, M. H., J. L. Lin, R. T. Cederwall, J. J. Yio, and S. C. Xie (2001), Objective analysis of ARM IOP data: Method and sensitivity, *Mon. Weather Rev.*, *129*, 295–311.
-
- U. Lohmann, Institute for Atmospheric and Climate Science, Eidgenössische Technische Hochschule (ETH), CH-8093 Zurich, Switzerland.
- P. Stier, Max Planck Institute for Meteorology, Bundesstrasse 53, D-20146 Hamburg, Germany.
- J. Zhang, Modelling and Integration Division (ARQI), Air Quality Research Branch, Meteorological Service of Canada, 4905 Dufferin Street, Downsview, ON M3H 5T4, Canada. (junhua.zhang@ec.gc.ca)